



Supernovae within Pre-existing Wind-blown Bubbles: Dust Injection versus Ambient Dust Destruction

Sergio Martínez-González¹ , Richard Wunsch² , Sergiy Silich³ , Guillermo Tenorio-Tagle³ , Jan Palouš² , and Andrea Ferrara⁴ 

¹ CONACYT–Instituto Nacional de Astrofísica, Óptica y Electrónica, AP 51, 72000 Puebla, Mexico; sergiomt@inaoep.mx

² Astronomical Institute, Czech Academy of Sciences, Boční II 1401/1, 141 00 Praha 4, Czech Republic

³ Instituto Nacional de Astrofísica, Óptica y Electrónica, AP 51, 72000 Puebla, Mexico

⁴ Scuola Normale Superiore, Piazza dei Cavalieri 7, I-56126 Pisa, Italy

Received 2019 September 12; revised 2019 November 5; accepted 2019 November 11; published 2019 December 19

Abstract

By means of 3D hydrodynamical simulations, we evaluate here the impact that supernova (SN) explosions occurring within wind-driven bubbles have on the survival or destruction of dust grains. We consider both the dust generated within the ejecta and the dust initially present in the ambient gas and later locked up in the surrounding wind-driven shell (WDS). The collision of the SN blast wave with the WDS leads to a transmitted shock that moves into the shell and a reflected shock that moves into the ejecta. The transmitted shock is capable of destroying large amounts of the dust locked in the shell, but only if the mass of the WDS is small, less than a few tens the ejected mass. Conversely, massive WDSs, with several times the ejected mass, lead upon the interaction to strong radiative cooling, which inhibits the Sedov–Taylor phase and weakens the transmitted shock, making it unable to traverse the WDS. In such a case, the destruction/disruption of the ambient dust is largely inhibited. On the other hand, the SN remnants grow rapidly in the very tenuous region excavated by the stellar winds, and thus a large fraction of the dust generated within the ejecta is not efficiently destroyed by the SN reverse shock, nor by the reflected shock. Our calculations favor a scenario in which core-collapse SNe within sufficiently massive WDSs supply more dust to the interstellar medium than they are able to destroy.

Unified Astronomy Thesaurus concepts: [Supernova remnants \(1667\)](#); [Interstellar dust \(836\)](#); [Interstellar medium \(847\)](#); [Chemical enrichment \(225\)](#); [Dust shells \(414\)](#); [Hydrodynamics \(1963\)](#); [Hydrodynamical simulations \(767\)](#); [Stellar winds \(1636\)](#); [Circumstellar shells \(242\)](#)

1. Introduction

The propagation of supernova (SN) blast waves through their surrounding medium is held responsible for inducing the disruption (via grain shattering) and destruction (via thermal and kinetic sputtering) of a large mass of swept-up interstellar dust (Jones et al. 1996; Slavin et al. 2015). On the other hand, while core-collapse SNe are recognized as efficient dust producers (e.g., Todini & Ferrara 2001; Indebetouw et al. 2014; Matsuura et al. 2015), several authors have argued that a large fraction of their ejecta dust will be returned to the gas phase during the thermalization of the SN ejecta (e.g., Nozawa et al. 2007; Bocchio et al. 2016; Martínez-González et al. 2016, 2017; Micelotta et al. 2016). It is therefore natural to ask whether SNe are ultimately net producers or destroyers of dust, and under which conditions the answer could be one or the other.

Aiming to answer this question, Lakićević et al. (2015) have asserted that SNe in the Large Magellanic Cloud (LMC) have sputtered more ambient dust than they were able to produce. Their conclusion is based on the analysis of maps of far-infrared and submillimeter dust temperature and dust mass in and around several SN remnants (SNRs). However, they were unable to determine whether the dust grains were mostly destroyed or displaced and piled-up. A similar conclusion was drawn by Temim et al. (2015), who inferred the amount of dust sputtered by individual SN blast waves and the global rate of grain destruction in the Magellanic Clouds using observationally derived values of the ambient gas density and dust-to-gas mass ratio around individual SNRs. However, massive stars produce vigorous stellar winds prior to their explosion, and the

role of a pre-existing wind-blown bubble in the survival/destruction of interstellar grains has not been considered in sufficient detail.

The stellar wind produced by a massive star (or a collection of them) piles up the surrounding ambient gas into a thin, quickly cooling, expanding shell. The medium surrounding the massive star is then structured (from the center outward) into a free-wind region, a shocked-wind region separated from a wind-driven shell (WDS) by a contact discontinuity, and the surrounding undisturbed ambient medium.

As the massive star explodes, and upon collision of the SN blast wave with the encompassing WDS, a reflected shock and a transmitted shock are generated (Tenorio-Tagle et al. 1990, 1991; Franco et al. 1991; Różyczka et al. 1993). The crucial factor determining the strength of the shocks is the ratio between the amount of mass collected by the WDS and the mass of the SN ejecta ($\chi = M_{\text{wds}}/M_{\text{ej}}$). For WDSs with⁵ $\chi \lesssim 40$, the SN blast wave rams through and further compresses the WDS and continues to sweep up the unperturbed interstellar medium. In contrast, if $\chi \gtrsim 40$, the transmitted shock is unable to overrun the WDS and the ambient medium ahead of it remains largely undisturbed. These results were later confirmed by Dwarkadas (2005, 2007) and by van Marle et al. (2015) and Haid et al. (2016).

Tenorio-Tagle et al. (1990) also found that the SNR–WDS interaction is expected to trigger an order-of-magnitude rise in

⁵ The limiting value of $\chi \approx 40$, which determines whether the SN blast wave is able to overrun a WDS, was calculated for a 10^{51} erg explosion with ejecta mass equal to $4 M_{\odot}$.

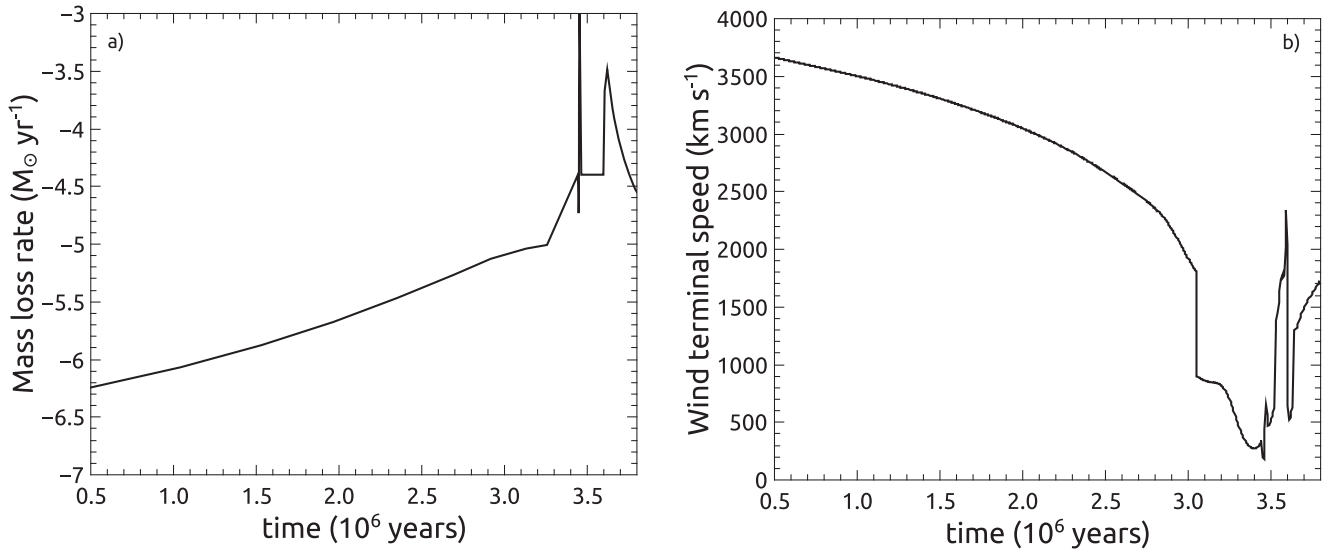


Figure 1. (a) Evolution of the mass loss rate for a $60 M_{\odot}$ star with solar metallicity obtained by Schaller et al. (1992). (b) Corresponding evolution of the terminal speed assuming the conversion factor between v_{∞} and v_{esc} introduced by Vink et al. (2001).

the X-ray emission. In fact, it has been claimed that the LMC’s SNRs N63A, N132D, and N49B have exploded within a wind-blown bubble given their X-ray appearance (Hughes et al. 1998).

Here we focus on single massive stars that are immersed in wind-driven bubbles (WDBs) prior to their final core-collapse. By performing three-dimensional hydrodynamical simulations, we model the collision of an SN blast wave with the pre-existing WDS and then determine the amount of pre-existing ambient dust that is destroyed during the pre-SN WDB expansion and after the development of the reflected and transmitted shocks. The crucial parameter is the mass ratio between the WDS and the SN ejecta, so we fix the parameters related to the stellar wind and the SN explosion while varying the mass of the WDS and the density of the ambient medium.

The paper is organized as follows: Section 2 describes our physical and computational scheme, the initial setup (Section 2.1), the stellar wind properties (Section 2.2), and the SN properties (Section 2.3). In Section 3 we discuss the case of SNe evolving in uniform, homogeneous media, while Section 4 focuses on the more realistic case of SNe occurring within an encompassing WDS. In Section 5 we outline our major conclusions.

2. Model Setup

We have run a set of three-dimensional hydrodynamical simulations with the adaptive mesh refinement code FLASH v4.3 (Fryxell et al. 2000) to explore the explosion of individual massive stars in homogeneous media and within wind-blown bubbles. The hydrodynamic equations are solved with a modified version of the piecewise parabolic method (Colella & Woodward 1984) and the scheme takes into account the equilibrium cooling function of optically thin plasmas (Schure et al. 2009) and the cooling induced by gas–grain collisions (calculated using the CINDER module: Martínez-González et al. 2018, hereafter MWP+18). With CINDER we also calculate on-the-fly the rate of thermal sputtering given the initial distribution of grain sizes and dust mass. Our scheme considers the action of thermal sputtering during the whole evolution of the WDS and the subsequent SNR and assumes a tight coupling between gas

and dust. We have generated random initial density perturbations (white noise) in order to emulate a degree of clumpiness in the SN ejecta. All the simulations were performed in a uniform grid (256^3 and 512^3 , as specified later).

2.1. Properties of the Ambient Medium

The simulations are initialized in a dusty medium with a constant gas number density, n_a , gas temperature, T_a , and dust-to-gas mass ratio, \mathcal{D}_a . A gas with one helium atom for every ten hydrogen atoms was considered in all the simulations, corresponding to a mean mass per particle of ionized and neutral gas $\mu_i = \frac{14}{23}m_H$ and $\mu_n = \frac{14}{11}m_H$, respectively, where m_H is the proton mass.

Since stars on the asymptotic giant branch and SNe II-P (which are the majority of core-collapse SNe: Sukhbold et al. 2016) tend to form preferentially large (and long-lived) dust grains (Todini & Ferrara 2001; Nozawa et al. 2003; Kozasa et al. 2009; Asano et al. 2013), the ambient grain population is chosen to follow a distribution of the form $\sim a^{-1} \exp\{-0.5[\log(a/a_0)/\sigma]^2\}$, with $a_0 = 0.1 \mu\text{m}$, $\sigma = 0.7$, and lower and upper limits $a_{\text{min}} = 0.01 \mu\text{m}$ and $a_{\text{max}} = 0.5 \mu\text{m}$, respectively, with equal fractions of silicate and carbonaceous grains. The grain mass densities, ρ_{gr} , are taken as 2.26 and 3.3 g cm^{-3} for silicate and carbonaceous grains, respectively. The grain size distribution is sampled using 10 logarithmically spaced bins (see also Appendix A in MWP+18).

2.2. Properties of the Stellar Wind and WDS

In order to model an isotropic stellar wind we have used the outputs of the stellar evolutionary models by Schaller et al. (1992), which span from the beginning of the hydrogen-burning phase to core-carbon exhaustion. We use, in particular, their time-dependent mass loss rate, $\dot{M}_w(t)$, bolometric luminosity, $L_{\text{bol}}(t)$, and effective temperature, $T_{\text{eff}}(t)$, for stars with a solar composition. With these values, the effective stellar radius, $R_{\text{eff}}(t)$, escape velocity, $v_{\text{esc}}(t)$, and stellar wind terminal speed, $v_{\infty}(t)$, can be derived (assuming a conversion factor $v_{\infty} = 1.3v_{\text{esc}}$ if $T_{\text{eff}} < 27,000 \text{ K}$ and $v_{\infty} = 2.6v_{\text{esc}}$ if $T_{\text{eff}} \geq 27,000 \text{ K}$ (Vink et al. 2001; Szécsi & Wünsch 2019)).

Figure 1 shows the evolution of \dot{M}_w and v_∞ adopted in our stellar wind model.

We have used a modified version of the implementation of a time-dependent wind source by Wunsch et al. (2008). This approach inserts the wind into a small sphere with radius R_v , where the wind mass flux is

$$\dot{M}(r) = \dot{M}_w r / R_v. \quad (1)$$

The gas density and velocity around the source are reset at each time step as

$$\rho(r) = \frac{\dot{M}_w}{(4\pi v_\infty r^2)} \quad (2)$$

and

$$v(r) = v_\infty r / R_v, \quad (3)$$

where r is the distance of a grid cell from the source center.⁶ In addition, the temperature of the wind is set to a constant value of 10^4 K. The radius of the source R_v is a free parameter taken as small as possible.⁷

We have not modeled photoionization nor included the effects of radiation pressure on the dynamics and inner structure of the WDS (e.g., Martínez-González et al. 2014). We have also not considered any dust produced in stellar winds; however, under certain conditions the outflows of massive stars may produce copious amounts of dust prior to their explosion (see Kochanek 2011). This is particularly so in the case of colliding stellar winds in close massive binary systems, in eruptive events in luminous blue variables such as η Car (Gomez et al. 2010), and in the extremely dense ($\sim 10^{10}$ cm⁻³), post-shock cooling layers that result from the interaction of an SNR with a very dense and slow stellar wind (Smith 2017).

2.3. SN Properties

As the central massive star explodes, it expels a certain amount of mass, M_{ej} , whose kinetic energy is E_{SN} . We take progenitor-dependent values from Sukhbold et al. (2016) and insert them into a sphere of radius R_{SN} .⁸ The ejecta is composed of gas and dust. The selected initial radial profiles of the ejecta gas density and velocity are (Tang & Chevalier 2017)

$$\rho_{ej} = \frac{(3-n)}{4\pi} \frac{M_{ej}}{R_{SN}^3} \left(\frac{R_{SN}}{r} \right)^n \quad (4)$$

and

$$v_{ej} = \left(2 \frac{(5-n)}{(3-n)} \frac{E_{SN}}{M_{ej}} \right)^{1/2} \left(\frac{r}{R_{SN}} \right), \quad (5)$$

where r is a radial distance. We have taken $n = 2$ in all our simulations because other values of n have been shown not to alter significantly the evolution of the SNR (see Appendix B in MWP+18). At the time of insertion, the ejecta is assumed to be at 10^4 K.

⁶ r has been corrected so that it cannot be smaller than the size of a grid cell.

⁷ R_v was selected as 0.5 pc in our simulations, which permits an approximately spherical bubble with the adopted spatial resolution.

⁸ Similarly to the chosen value of R_v , $R_{SN} = 0.5$ pc is taken in our simulations.

3. Explosions in Uniform, Homogeneous Media

We have considered a set of cases with and without pre-existing WDBs. In this section we focus on the latter cases considering SN explosions occurring in ambient media with constant temperatures ($T_a = 10$ K), dust-to-gas mass ratios ($\mathcal{D}_a = 0.01$), and gas number densities, n_g . The homogeneous low-density case (SNa) has $n_a = 1$ cm⁻³ and the homogeneous high-density case (SNb) assumes $n_a = 1000$ cm⁻³. For these cases we selected a $60 M_\odot$ massive star that expels $M_{ej} = 5.58 M_\odot$ (5.08 M_\odot of gas and 0.5 M_\odot of dust) and $E_{SN} = 9.12 \times 10^{50}$ erg when it explodes as an SN. The size of the computational domain was selected to be (20 pc)³ and (10 pc)³ for SNa and SNb, respectively, both in a grid of 512^3 . Figure 2 shows the evolution of the dust mass of the SN ejecta and the mass of the ambient dust that is destroyed by the SN blast wave for (a) SNa and (b) SNb. For SNa the SN reverse shock takes ~ 5300 yr to propagate through the whole SN ejecta. At this time 0.25 M_\odot of ejecta dust and 0.88 M_\odot of ambient dust have been destroyed. The reverse shock bounces back upon arriving at the SNR's center and subsequently catches up and merges with the blast wave (Tenorio-Tagle et al. 1990; MWP+18). The diameter of the SNR grows to the size of the computational domain after ~ 6100 yr, when 1.2 M_\odot of ambient dust and 0.16 M_\odot of ejecta dust have been destroyed.

For the second model (SNb, see panel (b) in Figure 2), the whole amount of dust injected by the SN is destroyed within the reverse shock crossing time (~ 500 yr). Owing to the higher frequency of ion–grain collisions in the dense shell of swept-up ambient material, $\sim 1.6 M_\odot$ of ambient dust is destroyed within ~ 750 yr after the explosion. At this time, radiative cooling (aided by that induced by gas–grain collisions) in the shell of swept-up matter becomes catastrophic (the gas temperature drops drastically to $\lesssim 10^4$ K) and nearly terminates thermal sputtering. In total, 2.35 M_\odot of (ambient+ejecta) dust was destroyed.

In these cases, even without accounting for other destructive/disruptive processes, dust destruction easily overtakes dust production, as suggested by Lakićević et al. (2015), Temim et al. (2015), and Slavin et al. (2015). Additionally, in both cases the inclusion of dust-induced radiative cooling provokes a noticeable departure from the classical Sedov–Taylor (ST) solution as it dominates over the optically thin radiative cooling of shocked plasmas at temperatures $\gtrsim 3 \times 10^5$ K. Therefore, the ratios of kinetic energy and thermal energy to E_{SN} in case SNa reach only $E_k/E_{SN} \approx 0.25$ and $E_{th}/E_{SN} \approx 0.6$, respectively, once the whole ejecta is thermalized,⁹ (see panel (c) in Figure 2). Case SNb, which cools catastrophically and ceases dust destruction rapidly, shows a larger departure from the ST solution (panel (d) in Figure 2) as $\sim 90\%$ of E_{SN} is radiated away within a few thousand years. A “dustless” adiabatic case, similar to case SNa but with $\mathcal{D}_a = 0$ and a dust-free SN ejecta, was run and we obtained a good agreement with the adiabatic ST solution $E_k/E_{SN} \sim 0.32$ and $E_{th}/E_{SN} \sim 0.68$ once the whole SN ejecta is thermalized.

4. Explosions within WDBs

We now focus on the explosion of $60 M_\odot$ stars occurring within wind-blown bubbles. This choice is justified because SN metal and dust enrichment is particularly important at early cosmic times, before evolved stars start to contribute, and when

⁹ In the classical adiabatic ST solution (Sedov 1959) these values reach $E_k/E_{SN} \approx 0.3$ and $E_{th}/E_{SN} \approx 0.7$, respectively.

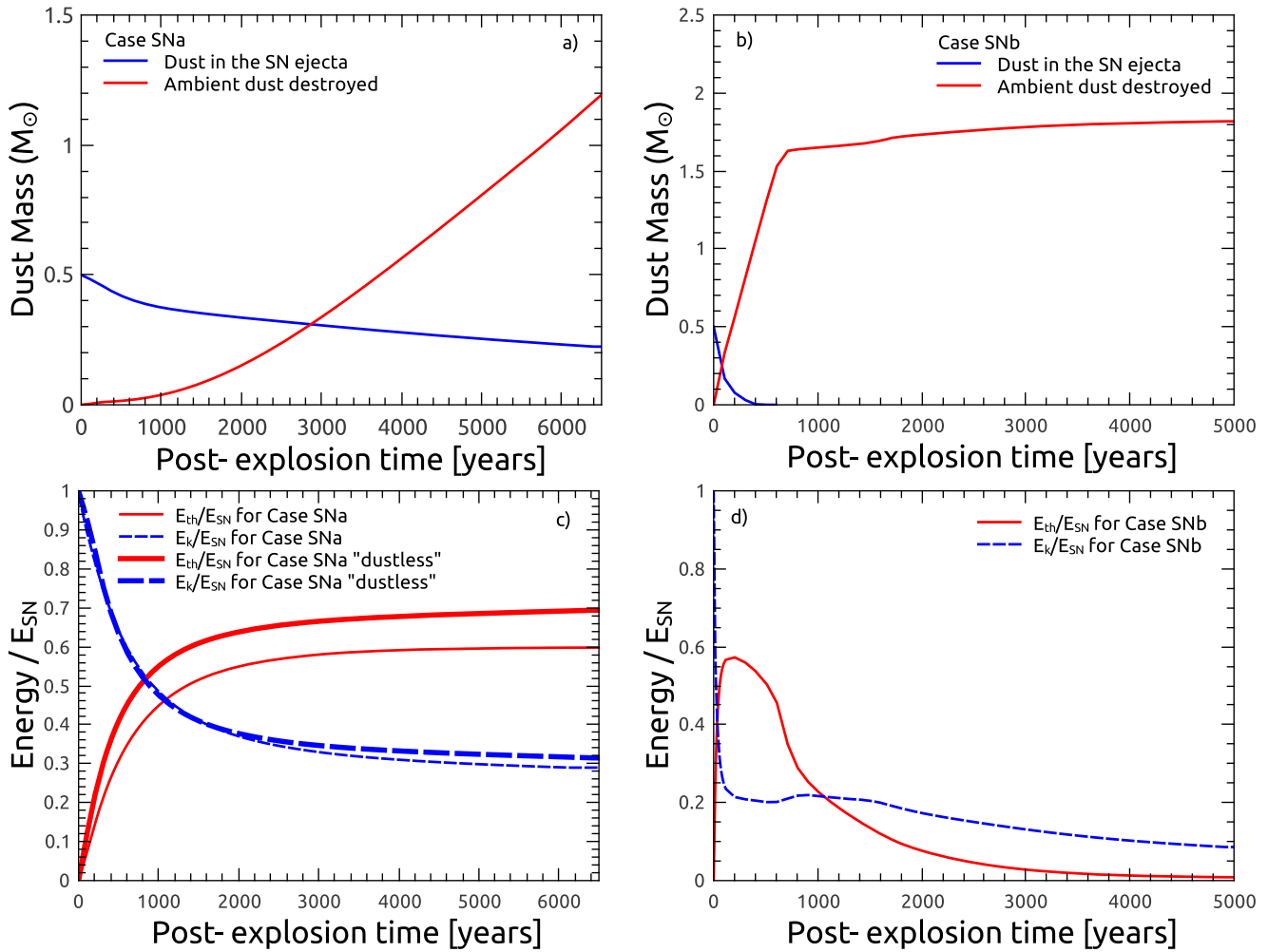


Figure 2. Explosions in homogeneous media. The upper panels show the evolution of the dust mass of the SN ejecta (blue lines), subject to reverse shock processing, and the mass of ambient dust destroyed by the SN blast wave (red lines) in the case of explosions occurring in homogeneous ambient media (for (a) SNa and (b) SNb, see Table 1). The lower panels present the fractions of kinetic energy (thin dashed blue lines) and thermal energy (thin solid red lines) for (c) SNa and (d) SNb. Additionally, panel (c) also displays these fractions for the “dustless” case using thicker lines.

the initial mass function is thought to be top-heavy (e.g., Schneider et al. 2002). Nevertheless, we do not expect a qualitatively large difference when studying other progenitor masses given that the crucial parameter that determines the SNR evolution, as found by Tenorio-Tagle et al. (1990), is the ratio of the WDS mass to the ejected mass. Indeed, van Marle et al. (2015), Dwarkadas (2007), and Haid et al. (2016) explored SNR–WDS collisions in the case of $40 M_{\odot}$, $30 M_{\odot}$, and $20 M_{\odot}$ progenitor stars, respectively, and confirmed the evolutionary trends found by Tenorio-Tagle et al. (1990).

For the purpose of studying bubbles evolving in low-density ambient media ($n_a = 1 \text{ cm}^{-3}$), and in order to maintain a sufficient spatial resolution, we have defined (see Table 1) a “low-mass WDS” case (WDBa) in which the central massive star explodes at an arbitrarily short time (1 Myr), i.e., a shorter time than the predicted evolution for a $60 M_{\odot}$ star. The mass of the WDS implies a value of $\chi \approx 400$. In this case, only $0.04 M_{\odot}$ of the dust present in the WDS is destroyed prior to the SN explosion (see Appendix A.1).

Before the collision of the SNR–WDS, and as the SNRs evolve in the tenuous region excavated by the stellar winds, only a small fraction of the SN ejecta is thermalized by the

Table 1
Summary of Results

Model	n_a (cm^{-3})	χ	M_d^{ej} (M_{\odot})	M_d^a (M_{\odot})
SNa	1	0	>0.34	$\gg 1.2$
SNa “dustless”	1	0
SNb	10^3	0	0.5	2.35
WDBa	1	400	0.02	~ 0.45
WDBb	10^3	2×10^4	0.025	0.28

Note. The table presents a summary of our results for each model according to the ambient gas number density and the ratio between the mass of the WDS and that of the SN ejecta at the time the massive star explodes. M_d^{ej} and M_d^a stand for the mass of ejecta and ambient dust, respectively, destroyed in each case.

reverse shock and about $\sim 4\%$ ($\sim 0.02 M_{\odot}$) of the ejecta dust is destroyed in case WDBa.

In this case, the SNR–WDS collision occurs about ~ 3200 yr after the SN explosion. The left panels in Figure 3 show the distribution of the gas number density, temperature, and dust density in the wind-blown bubble at a stellar evolutionary time

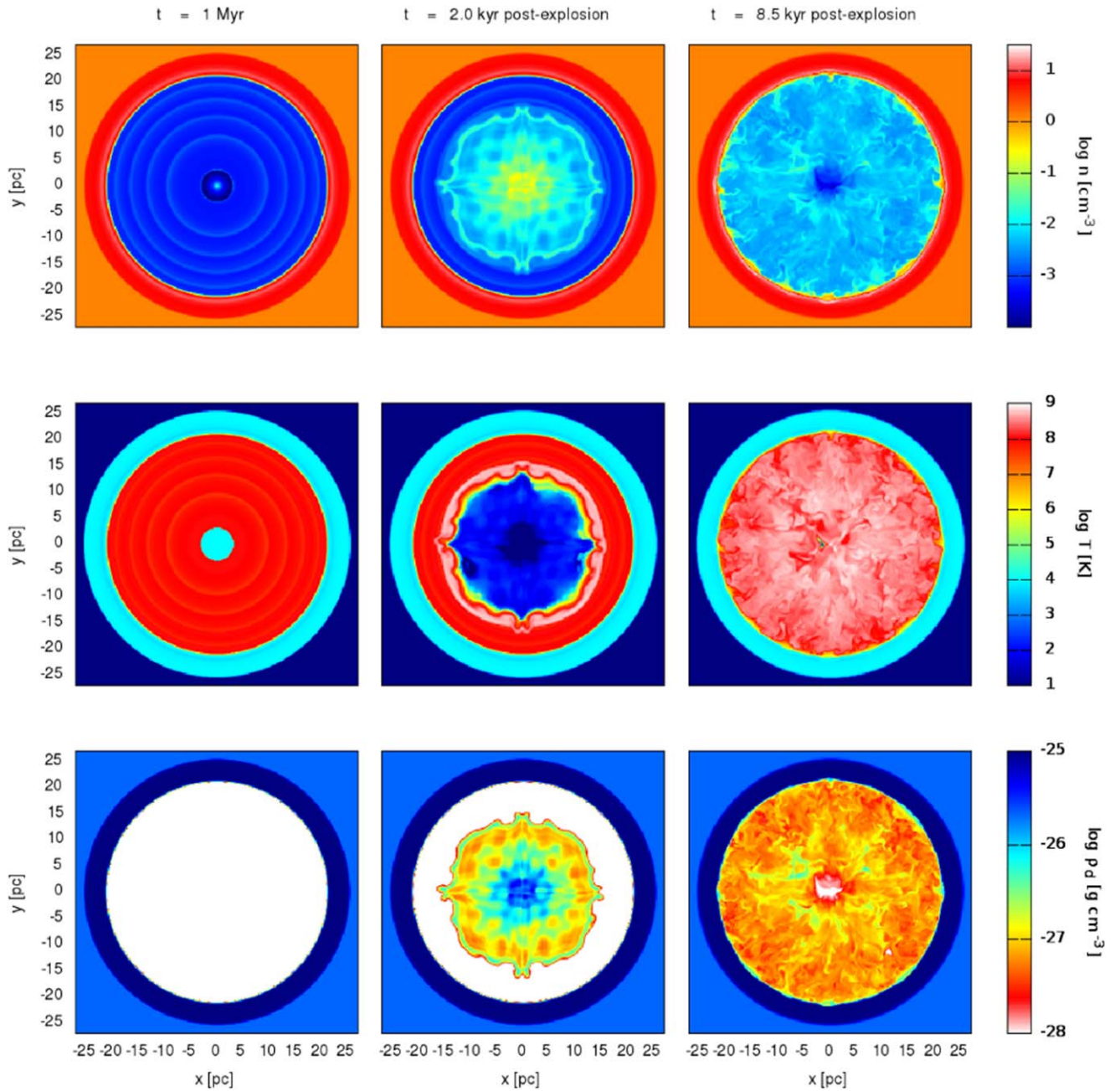


Figure 3. SN explosion within a wind-driven bubble in case WDBa. Two-dimensional cuts along the x - y plane ($z = 0$) of the distribution of gas number density (upper panels), gas temperature (middle panels), and dust mass density, $\rho_{d,s}$ (bottom panels) at 1 Myr into the evolution of the stellar wind (left panels), and at 2000 yr after the explosion (middle panels) and 8500 yr after it (right panels). After the SNR–WDS collision, the SN ejecta recoils and fills the wind/SNR, and the gas density and temperature start to even out. The dust density in the wind/SNR drops mostly because of the SNR expansion rather than because of grain destruction.

of 1 Myr for the WDBa case. Prior to the SN explosion, the WDB shows its four-zone structure and one can note the piling-up of the gas and dust in the WDS. The middle panels show the same quantities but 2000 yr after the SN explosion. At this time, the SNR is sweeping up the wind matter and the blast wave is approaching a collision with the WDS. When the SNR–WDS collision occurs, the reflected shock produced catches up and merges with the SN reverse shock, reaches the remnant’s center, and then transforms into a subsonic forward wave.

As illustrated in the right panels of Figure 3 for the WDBa case, the SN blast wave is unable to overrun the WDS, and the SNR ends up being confined to roughly the size that the WDB had reached at 1 Myr. This is also the case at higher ambient

densities and when the SN explosion takes place at later times (see Figure 4). Panel (a) in Figure 5 shows that the WDS, allowed to evolve for only 1 Myr, is massive enough to prevent the blast wave from destroying a larger mass of dust than that able to survive in the SN ejecta.

Limited spatial resolution inhibits a complete calculation of a low-density case in which we could follow the full evolution of the WDB over 3.8 Myr. This is due to the very large radius that the bubble would acquire, which would prevent us from sufficiently resolving the early stages of the SNR evolution. However, it can be envisaged that an even smaller amount of ambient dust would be destroyed if the blast wave were to encounter an even more massive WDS than in case WDBa (see Table 1).

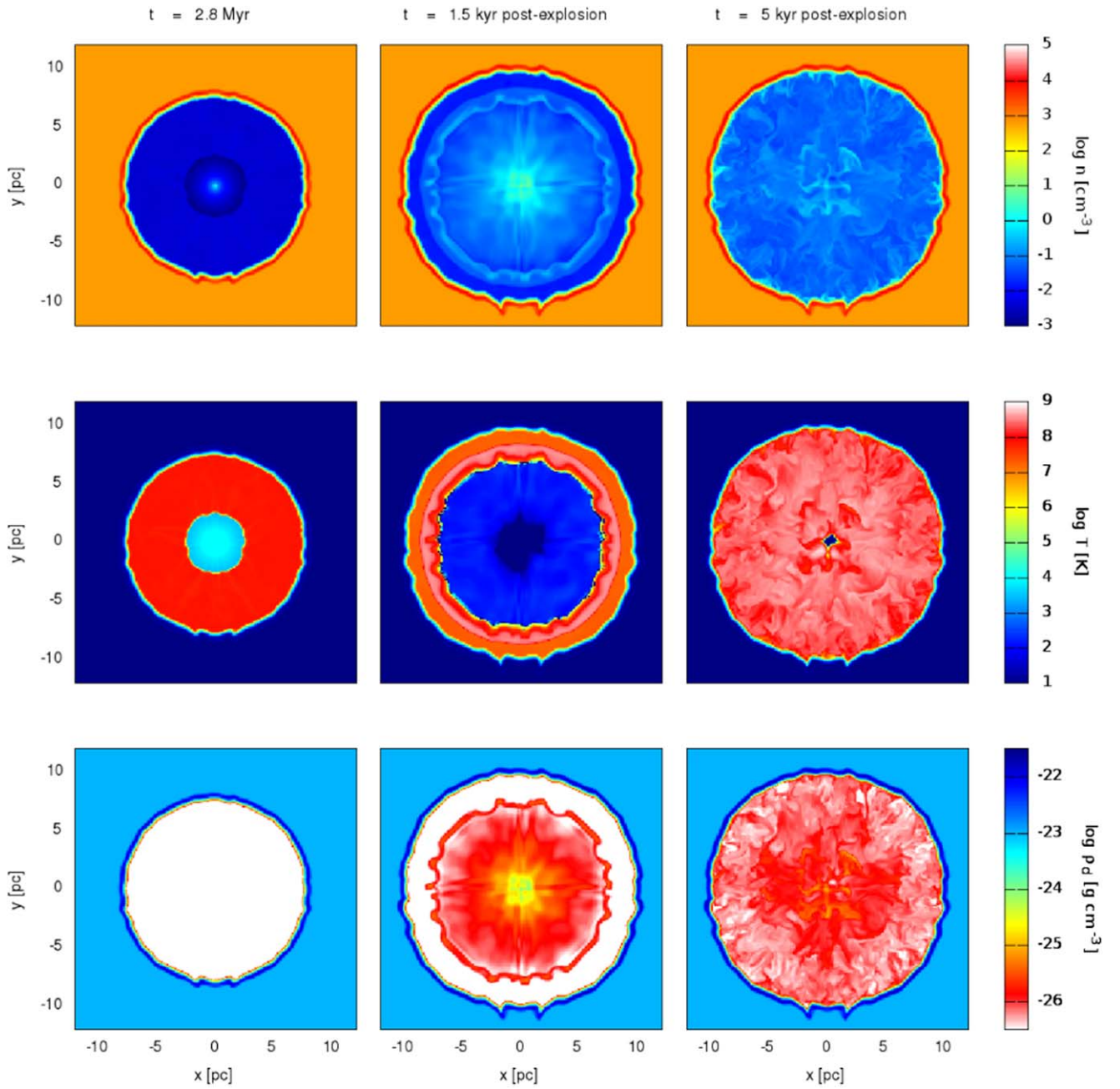


Figure 4. Same as Figure 3 but for the WDBb case at 2.8 Myr into the evolution of the stellar wind (left panels), and at 1500 yr after the explosion (middle panels) and 5000 yr after it (right panels).

We have also studied a high-density case (WDBb, $n_a = 1000 \text{ cm}^{-3}$), in which we let the massive star inject its stellar wind until core-carbon exhaustion occurs, given that the final core-collapse will proceed shortly afterward ($\sim 3.8 \text{ Myr}$). This simulation is inscribed into a cube of $(54 \text{ pc})^3$ in a grid 256^3 .

Upon the SNR–WDS collision, the transmitted shock moves initially at a velocity of a few thousand km s^{-1} . However, at 3.8 Myr the massive WDS is four orders of magnitude more massive than the SN ejecta and thus this velocity cannot be sustained for a long distance and drops sharply (Dwarkadas 2007). This also limits the relative importance of other grain disruption mechanisms that require high-velocity shock processing (e.g., kinetic sputtering and grain shattering, see Appendix A.2).

As depicted in panel (a) in Figure 5, only $\sim 5\%$ ($0.025 M_\odot$) of the dust mass injected by the SN is destroyed. Not only that,

but about $\sim 0.28 M_\odot$ of ambient dust is destroyed ($\sim 0.025\%$ of the total amount of swept-up ambient dust). Thus, in both cases WDBa and WDBb, the massive WDS poses an almost insurmountable barrier that prevents the SN blast wave from processing the majority of the ambient dust locked in the WDS.

In both WDB cases, the ST phase is totally inhibited by strong radiative cooling, which becomes dominant early on in the SNR evolution. Therefore, the energy of the SN explosion is quickly radiated away rather than used to sustain thermal collisions of gas and dust (see panel (c) in Figure 5 for the WDBb case).

As envisaged by Doroshenko et al. (2016), the survival of ejecta dust is favored because of the SNR expansion within the low-density medium excavated by the stellar wind, similarly to what was found by MWP+18 for the case of clustered SNe evolving in a collective star cluster wind. On top of that, kinetic

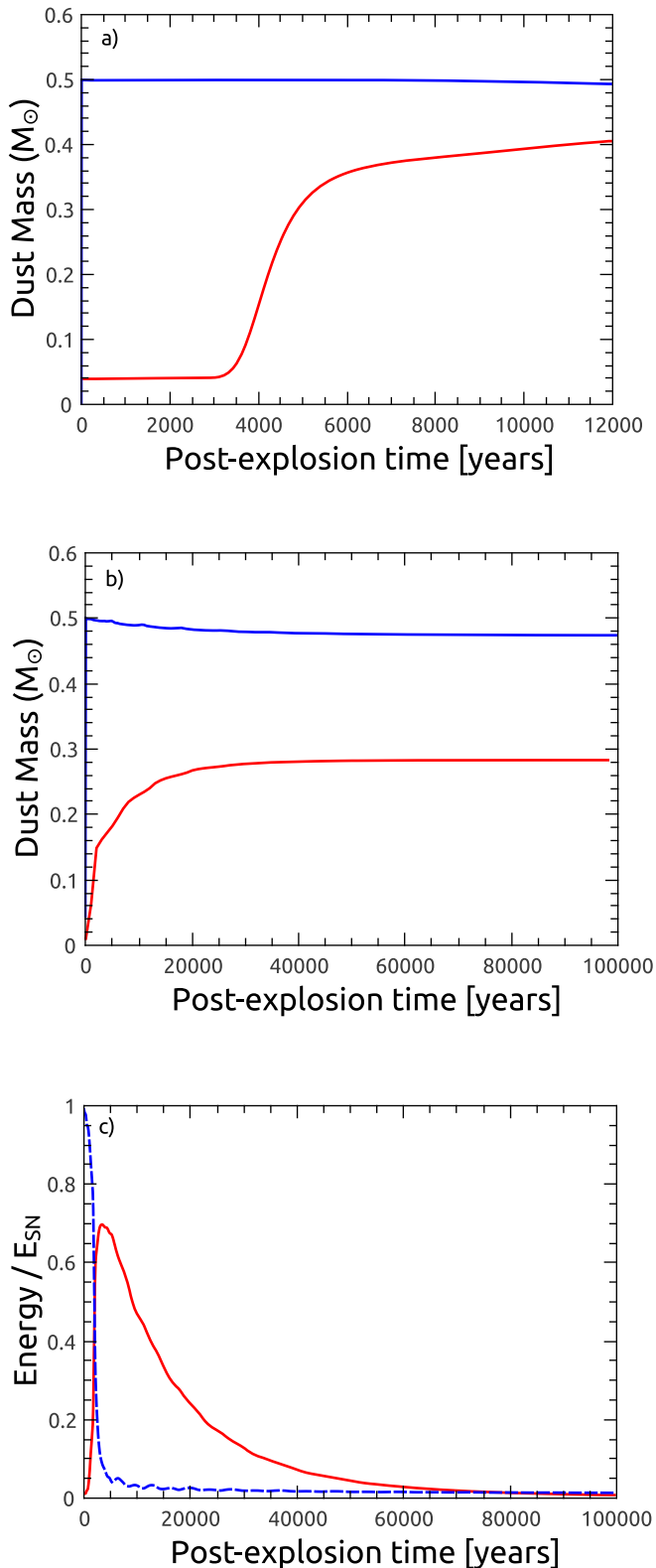


Figure 5. Explosions within wind-driven bubbles. Panels (a) and (b) depict the evolution of the dust mass of the SN ejecta (blue lines) and the mass of ambient dust destroyed by the leading and transmitted SN blast waves (red lines) in the case of explosions occurring within wind-blown bubbles. Panel (a) shows the lines corresponding to WDBa and panel (b) those for WDBb (see Table 1). Panel (c) presents the fractions of kinetic energy (blue dashed lines) and thermal energy (red solid lines) for the SNR in case WDBb (see also panel (d) in Figure 2).

sputtering and grain shattering (not included in our simulations) will most likely be disfavored given that they also require a sufficient rate of gas–grain and grain–grain encounters and not just a large relative motion between impinging particles/grains (see Appendix A.2). As a result, the consideration of the full stellar mass-loss history has a profound impact on the survival of both the ambient and the ejecta dust grains.

Note also that the presence of regions of low dust density around SNRs does not necessarily imply, as previously suggested, that core-collapse SNe destroy more dust than they produce (see bottom panels in Figures 3 and 4). Moreover, the SN ejecta dust will mostly radiate at near- to mid-infrared wavelengths, and therefore will be more difficult to observe in far-infrared and submillimeter maps.

We have neglected the presence of interstellar magnetic fields, which can increase the thickness of the WDS as it re-expands driven by magnetic pressure, thus decreasing its density (Ferriere et al. 1991). In that scenario, the transmitted shock could propagate farther into the WDS than in the absence of a magnetic field. However, not only the gas density but also the dust density is reduced, and thus the timescale for grain destruction within the WDS is increased ($\tau_{\text{dest}} \sim n^{-1}$) (see also van Marle et al. 2015, who showed that even in the presence of a strong interstellar magnetic field, an SN blast wave is still unable to overrun its encompassing massive WDS). Thus, the presence of an interstellar magnetic field is unlikely to change our conclusions significantly.

5. Concluding Remarks

Previous studies have estimated that SN explosions in homogeneous ambient media destroy more dust than SNe are able to inject (e.g., Lakićević et al. 2015; Slavin et al. 2015; Temim et al. 2015). However, these estimates did not take into consideration the shaping of the interstellar gas during the pre-SN evolution of the massive star. During this stage, powerful stellar winds evacuate the ambient gas from the stellar vicinity, compressing it into an expanding dense shell. This may affect the SNR evolution significantly.

Indeed, as shown by Tenorio-Tagle et al. (1990) and Franco et al. (1991), an SN blast wave is able to overrun an encompassing WDS only if its mass, M_{wds} , is small and comparable to the mass of the SN ejecta, M_{ej} . In the other case, when $M_{\text{wds}} \gg M_{\text{ej}}$, the WDS becomes an insurmountable barrier that confines the SNR within the WDB.

Here we have shown, by means of three-dimensional hydrodynamical simulations, that this also affects the fate of pre-existing ambient and SN ejecta dust grains. The ambient dust grains accumulated in a massive WDS remain largely unaffected by thermal sputtering after the SNR–WDS collision. The dust ejected by SNe is also mostly unaffected as the SNRs expand rapidly in the tenuous region previously excavated by the pre-existing stellar wind. Destruction of ejecta dust in such cases is caused by the reflection of the blast wave that catches up with the reverse shock rather than by the passage of the reverse shock alone. In these cases, radiative cooling proceeds very rapidly and the SNRs do not pass through the ST phase. Other grain destructive/disruptive processes are expected to also be inhibited in the WDS because the transmitted shock is weak and penetrates only into a very thin inner layer of the WDS. This also prevents efficient mixing between the WDS matter and that from the wind/SNR.

This situation is radically different from that occurring when the explosion is modeled in a homogeneous medium or embedded in a low-mass WDS, where one can expect that the blast wave and the reverse shock could destroy far more dust than can be produced after the SN explosion.

This study, together with the three-dimensional hydrodynamical simulations for the case of clustered SNe presented by MWP+18, shows that core-collapse SNe may supply dust efficiently to the ambient medium and that they do not destroy large amounts of pre-existing dust in the surroundings. As the fraction of surviving ejecta dust might be very high, this result is also consistent with recent estimates of little dust destruction by SNe in the Local Group and in high-redshift galaxies (Gall & Hjorth 2018; Michałowski et al. 2019) and with theoretical expectations that suggest that the bulk of dust in the early universe must come from core-collapse SNe (Ferrara et al. 2016).

The authors thankfully acknowledge the computer resources, technical expertise, and support provided by the Laboratorio Nacional de Supercómputo del Sureste de México, CONACYT member of the network of national laboratories. This study was supported by CONACYT–México research grant A1-S-28458. S.M.G. also acknowledges support by CONACYT through Cátedra n.482. R.W. and J.P. acknowledge the support from project 19-15008S of the Czech Science Foundation and from the institutional project RVO:67985815 and the support by The Ministry of Education, Youth and Sports of the Czech Republic from the Large Infrastructures for Research, Experimental Development and Innovations project “IT4Innovations National Supercomputing Center LM2015070.” A.F. acknowledges support from the ERC Advanced grant INTERSTELLAR H2020/740120. Any dissemination of results must indicate that it reflects only the authors’ view and that the Commission is not responsible for any use that may be made of the information it contains. This research was supported by the Munich Institute for Astro- and Particle Physics (MIAPP) of the DFG cluster of excellence “Origin and Structure of the Universe.” Partial support from the Carl Friedrich von Siemens-Forschungspreis der Alexander von Humboldt-Stiftung Research Award is kindly acknowledged.

Appendix

A.1. Ambient Dust Processing during the Pre-SN Evolution

We have taken into consideration the action of thermal sputtering during the whole pre-SN evolution of the WDB. However, the ambient dust locked in the WDS is not significantly affected by thermal sputtering because the WDS cools down quickly to $\sim 10^4$ K.

This occurs in a timescale, τ_{cool} , approximately given by (Mac Low & McCray 1988)

$$\tau_{\text{cool}} = (2.3 \times 10^4) \left(\frac{Z_a}{Z_\odot} \right)^{-0.42} \left(\frac{n_a}{1 \text{ cm}^{-3}} \right)^{-0.71} \times \left(\frac{L_w}{10^{38} \text{ erg s}^{-1}} \right)^{0.29} \text{ yr}, \quad (6)$$

where Z_a is the metallicity and n_a is the density of the ambient medium, and $L_w = \frac{1}{2} \dot{M}_w v_\infty^2$ is the wind mechanical luminosity. For case WDBa, the WDS cools down in ~ 250 kyr, leading to

the destruction of only $0.01 M_\odot$ of the dust locked in the WDS. For case WDBb, the WDS cools down in less than ~ 2000 yr. These simple estimates of τ_{cool} ignore the contribution of dust grains to the cooling of the WDS; when taken into account (as in our numerical scheme and that of Everett & Churchwell 2010) these timescales are greatly reduced and therefore destruction of the ambient dust in the WDS is suppressed. Not only that, but in the low-density cases thermal sputtering also becomes inefficient as the number density inside the WDS is only a few particles per cm^{-3} .

A.2. The Role of Kinetic Sputtering and Grain Shattering

Our simulations have ignored some processes that can be important for grain destruction, i.e., kinetic sputtering and grain shattering as a result of grain–grain collisions. The disruption timescales via kinetic sputtering and grain shattering are (e.g., Hoang & Tram 2019)

$$\tau_{\text{sp}}^k = \frac{4a\rho_{\text{gr}}}{nm_H Y_{\text{sp}}^k v_{\text{gr}}} \quad (7)$$

and

$$\tau_{\text{gg}} = \frac{4a\rho_{\text{gr}} \mathcal{D}}{3nm_H \delta v}, \quad (8)$$

where n is the gas number density, Y_{sp}^k is the sputtering yield, v_{gr} is the relative speed between gas and dust grains, \mathcal{D} is the dust-to-gas mass ratio, and δv is the relative speed between colliding dust grains.

The upper panels in Figures 3 and 4 show that the density of the bulk of the SN ejecta drops to $n \sim 10^{-1} - 10^{-2} \text{ cm}^{-3}$ when it is crossed by the reverse/reflected shock. For characteristic values of $a = 0.01 \mu\text{m}$, $Y_{\text{sp}}^k = 0.1$ (Hoang & Lee 2019), ejecta dust-to-gas mass ratio $\mathcal{D} \approx 0.5/5.08 \sim 10^{-1}$, $\rho_{\text{gr}} = 3 \text{ g cm}^{-3}$, $v_{\text{gr}} = 175 \text{ km s}^{-1}$ (Fry et al. 2018), and $\delta v_{\text{gr}} = 20 \text{ km s}^{-1}$ (Hoang & Tram 2019), the disruption timescale due to kinetic sputtering is $\tau_{\text{sp}}^k \sim 1.4 - 14 \text{ Myr}$, and that corresponding to grain–grain collisions is $\tau_{\text{gg}} \sim 4 - 41 \text{ Myr}$. The timescale for grain damping by gas–grain collisions is (Hoang et al. 2012)

$$\tau_{\text{damp}} = \frac{a\rho_{\text{gr}}}{n} \left(\frac{8m_H k_B T}{\pi} \right)^{-1/2}, \quad (9)$$

where k_B is the Boltzmann constant and $T \sim 10^8 \text{ K}$ is the gas temperature. τ_{damp} is much shorter ($\sim 43 \text{ kyr}$) than τ_{ksp} and τ_{gg} , and thus these processes are not important for grains immersed into the shocked ejecta when the SNR evolves within a WDB.

In the case of ambient dust grains locked up in the WDS, the fact that the velocity of the transmitted shock drops sharply and goes quickly below the threshold shock velocity for grain shattering ($\sim 40 \text{ km s}^{-1}$, Jones et al. 1996) inhibits kinetic, thermal sputtering, and grain–grain collisions for the vast majority of the WDS.

ORCID iDs

Sergio Martínez-González  <https://orcid.org/0000-0002-4371-3823>

Richard Wunsch  <https://orcid.org/0000-0003-1848-8967>

Sergiy Silich  <https://orcid.org/0000-0002-3814-5294>

Guillermo Tenorio-Tagle  <https://orcid.org/0000-0003-4163-4969>

Jan Palouš  <https://orcid.org/0000-0001-6729-2851>

Andrea Ferrara  <https://orcid.org/0000-0002-9400-7312>

References

- Asano, R. S., Takeuchi, T. T., Hirashita, H., & Nozawa, T. 2013, *MNRAS*, **432**, 637
- Bocchio, M., Marassi, S., Schneider, R., et al. 2016, *A&A*, **587**, A157
- Colella, P., & Woodward, P. R. 1984, *JCoPh*, **54**, 174
- Doroshenko, V., Pühlhofer, G., Kavanagh, P., et al. *MNRAS*, **458**, 2565
- Dwarkadas, V. V. 2005, *ApJ*, **630**, 892
- Dwarkadas, V. V. 2007, *ApJ*, **667**, 226
- Everett, J. E., & Churchwell, E. 2010, *ApJ*, **713**, 592
- Ferrara, A., Viti, S., & Ceccarelli, C. 2016, *MNRAS*, **463**, L112
- Ferriere, K. M., Mac Low, M.-M., & Zweibel, E. G. 1991, *ApJ*, **375**, 239
- Franco, J., Tenorio-Tagle, G., Bodenheimer, P., & Rozyczka, M. 1991, *PASP*, **103**, 803
- Fry, B. J., Fields, B. D., & Ellis, J. R. 2018, arXiv:1801.06859
- Fryxell, B., Olson, K., Ricker, P., et al. 2000, *ApJ*, **131**, 273
- Gall, C., & Hjorth, J. 2018, *ApJ*, **868**, 62
- Gomez, H. L., Vlahakis, C., Stretch, C. M., et al. 2010, *MNRAS*, **401**, L48
- Haid, S., Walch, S., Naab, T., et al. 2016, *MNRAS*, **460**, 2962
- Hoang, T., Lazarian, A., & Schlickeiser, R. 2012, *ApJ*, **747**, 54
- Hoang, T., & Lee, H. 2019, arXiv:1909.07001
- Hoang, T., & Tram, L. N. 2019, *ApJ*, **877**, 36
- Hughes, J. P., Hayashi, I., & Koyama, K. 1998, *ApJ*, **505**, 732
- Indebetouw, R., Matsuura, M., Dwek, E., et al. 2014, *ApJL*, **782**, L2
- Jones, A. P., Tielens, A. G. G. M., & Hollenbach, D. J. 1996, *ApJ*, **469**, 740
- Kochanek, C. S. 2011, *ApJ*, **743**, 73
- Kozasa, T., Nozawa, T., Tominaga, N., et al. 2009, in ASP Conf. Ser. 414, Cosmic Dust—Near and Far, ed. T. Henning, E. Grün, & J. Steinacker (San Francisco, CA: ASP), 43
- Lakićević, M., van Loon, J. T., Meixner, M., et al. 2015, *ApJ*, **799**, 50
- Mac Low, M.-M., & McCray, R. 1988, *ApJ*, **324**, 776
- Martínez-González, S., Silich, S., & Tenorio-Tagle, G. 2014, *ApJ*, **785**, 164
- Martínez-González, S., Tenorio-Tagle, G., & Silich, S. 2016, *ApJ*, **816**, 39
- Martínez-González, S., Wunsch, R., & Palouš, J. 2017, *ApJ*, **843**, 95
- Martínez-González, S., Wunsch, R., Palouš, J., et al. 2018, *ApJ*, **866**, 40
- Matsuura, M., Dwek, E., Barlow, M. J., et al. 2015, *ApJ*, **800**, 50
- Micelotta, E. R., Dwek, E., & Slavín, J. D. 2016, *A&A*, **590**, A65
- Michałowski, M. J., Hjorth, J., Gall, C., et al. 2019, *A&A*, **632**, A43
- Nozawa, T., Kozasa, T., Habe, A., et al. 2007, *ApJ*, **666**, 955
- Nozawa, T., Kozasa, T., Umeda, H., Maeda, K., & Nomoto, K. 2003, *ApJ*, **598**, 785
- Rózyzka, M., Tenorio-Tagle, G., Franco, J., & Bodenheimer, P. 1993, *MNRAS*, **261**, 674
- Schaller, G., Schaerer, D., Meynet, G., & Maeder, A. 1992, *A&AS*, **96**, 269
- Schneider, R., Ferrara, A., Natarajan, P., & Omukai, K. 2002, *ApJ*, **571**, 30
- Schure, K. M., Kosenko, D., Kaastra, J. S., Keppens, R., & Vink, J. 2009, *A&A*, **508**, 751
- Sedov, L. I. 1959, *Similarity and Dimensional Methods in Mechanics* (New York: Academic)
- Slavin, J. D., Dwek, E., & Jones, A. P. 2015, *ApJ*, **803**, 7
- Smith, N. 2017, in *Handbook of Supernovae*, ed. A. Alsabti & P. Murdin (Cham: Springer), 403
- Sukhbold, T., Ertl, T., Woosley, S. E., Brown, J. M., & Janka, H.-T. 2016, *ApJ*, **821**, 38
- Szécsi, D., & Wunsch, R. 2019, *ApJ*, **871**, 20
- Tang, X., & Chevalier, R. A. 2017, *MNRAS*, **465**, 3793
- Temim, T., Dwek, E., Tchernyshyov, K., et al. 2015, *ApJ*, **799**, 158
- Tenorio-Tagle, G., Bodenheimer, P., Franco, J., & Rozyczka, M. 1990, *MNRAS*, **244**, 563
- Tenorio-Tagle, G., Rozyczka, M., Franco, J., & Bodenheimer, P. 1991, *MNRAS*, **251**, 318
- Todini, P., & Ferrara, A. 2001, *MNRAS*, **325**, 726
- van Marle, A. J., Meliani, Z., & Marcowith, A. 2015, *A&A*, **584**, A49
- Vink, J. S., de Koter, A., & Lamers, H. J. G. L. M. 2001, *A&A*, **369**, 574
- Wünsch, R., Tenorio-Tagle, G., Palouš, J., & Silich, S. 2008, *ApJ*, **683**, 683